POLITECNICO
MILANO 1863

SCUOLA DI INGEGNERIA INDUSTRIALE
E DELL'INFORMAZIONE

Executive Summary of the Thesis

Control of transition phases in rigid-wing airborne wind energy system

Laurea Magistrale in Automation and control Engineering - Ingegneria dell'automazione

Author: Pedro Pablo Mitidieri

Advisor: Prof. Lorenzo Mario Fagiano

Co-advisor:

Academic year: 2021-2022

1. Introduction

The present thesis tackles the study of an Airborne Wind Energy system, intending to propose a methodological approach to design the transition between one cycle of electricity production and the next.
To produce a methodological approach, it is necessary to look for critical parameters that will allow the transition to be done effectively. In order to accomplish that, a realistic model is developed, the different phases of the mission are studied and classified, and a control strategy is proposed. The last phase is the one where the main focus is placed. Finally, four key parameters remained, and a complete mission using them is presented. In addition, the explanation of their particular effects is added, along with a graphic representation of the transition modification when each one of them is changed.

2. System description and operating strategies

The kite(referred to as "drone" in the remained) under study is a quad-rotor fixed-wing hybrid, inspired by that of the company KIteMill AS[3]. It features a hybrid configuration with motors and wings with control surfaces. The analysis, modelling and design are made in continuous time for simplicity reasons, where the time variable is defined as $t \in R$.
The system is working in cross-wind for a critical reason, the effect of the freestream is constant during the whole operation. This provides a clear benefit, the lift is closer to being constant. As it is also much bigger than the weights of the different parts in this kind of system, the remaining force can be used to produce energy.

2.1. Operation scheme

In normal conditions, the system's working principle can be organized as follows. First, the vertical take-off. Then, the transition from hovering to power generation. The third part is where Power generation takes place. Afterward, there is the transition from flight to hovering. The final part is the vertical landing.

2.2. Coordinate systems

A range of coordinate systems is used to have an accurate and accessible description of the drone-tether-winch system.

1. **Earth frame**(ef): it is an inertial coordinate system commonly referred as NED co-

ordinate system.

2. **sphere coordinates**(sphere) : it is based on describing the drone position in spherical coordinates, $\theta_{sphere}(t)$ and $\phi_{sphere}(t)$.
3. **tether** : both the origin and the axis directions coincide with the ones explained before. Also, there is the definition of two rotations: $\phi_{tether}(t)$ (around N_{sphere}), $\theta_{tether}(t)$ (around E_{sphere}).

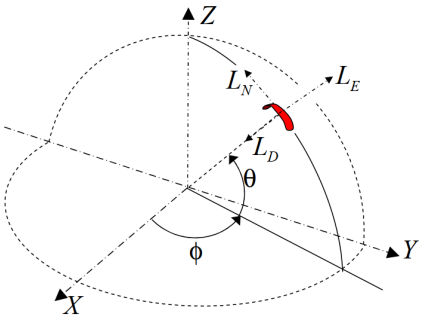

Figure 1: Sphere coordinates

4. **tether** : both the origin and the axis directions coincide with the ones explained before. Also, there is the definition of two rotations: $\phi_{tether}(t)$ (around N_{sphere}), $\theta_{tether}(t)$ (around E_{sphere}).
5. **body** (bf): it is the typical body coordinate system that defines body speeds (u(t), v(t) and w(t)) and the rotations $\phi(t)$, $\theta(t)$ and $\psi(t)$ (their derivatives are P(t), Q(t) and R(t), respectively).
6. **wind**(wf): The x-axis, in this case, has the same direction as the incoming wind, the z-axis points upwards, and the y-axis completes the trio.

The angles describing the airplane's attitude are used to create a new representation based on quaternions. It is used to overcome the singularity problem of the attitude's Euler-based representation.

3. Mathematical models

In this section, the mathematical models of the different components of the systems are presented. First, the tether model and its hypothesis are explained. Finally, the equations describing the behaviour of the drone are presented.

3.1. Tether model

A tether made of Dyneema sk78, a polymeric material, is assumed to be used in our system. The properties of this material are from [5]. It is assumed that the tether will have a diameter of 10 mm, which leads to a breaking load of 102 kN. In this work, it is decided to take a simple approach to the tether's modelling, a simple spring, joining the generator and the drone. As the generator unwinds the tether, the natural length of the spring is changed accordingly. The tether's parameters are K_{tether} = 2.366E+6 $\frac{N}{m}$ and ρ_{tether} = 975 $\frac{kg}{m^3}$.In this section, the mathematical models of the different components of the systems are presented. First, the tether model and its hypothesis are explained. Finally, the equations describing the behaviour of the drone are presented.

3.1.1 Tether forces

The force produced by the tether follows the simple equation describing a spring effect presented below. Where, $l_{tether}(t)$ is the length of the tether unwound and $l_{tether_0}(t)$ is the actual length of the tether.

$$F_{tether}(t) = max(0, K_{tether}(l_{tether}(t) - l_{tether_0}(t))) \quad (1)$$

As the tether is considered as a simple spring, the effect of its drag is considered using an approximation [4], presented below.

$$C_{D_{tether}} = \frac{C_{D_{cross-section}} d_{tether} l_{tether}(t)}{8S} \quad (2)$$

3.1.2 Length of the tether

For the sake of simplicity, it is considered that the controller of the winch system is fast enough to be regarded as instantaneous. As a result, the tether length is directly defined according to the strategy proposed in the following chapters.

3.2. Hybrid drone model

As it has been explained before, the drone modelled is a combination of a fixed-wing system with four rotors whose axis of rotation are always parallel to the z axis of the drone. First, the model of the system acting as a fixed-wing plane is studied, and then the model for the quadcopter behaviour is presented.

3.2.1 Aerodynamic forces and moments

The aerodynamic data for the *Kitemill* aircraft was taken from [2]. This information is used to approximate the aerodynamic coefficient of the drone in every instant, namely $C_D(t)$, $C_L(t)$, $C_Y(t)$, $C_m(t)$, $C_n(t)$ and $C_l(t)$.
Once the coefficients are obtained, the next step is to calculate the forces and moments derived from them. The aerodynamic forces are presented from (3b) to (3d), while the moments are presented from (3e) to (3f).

$$D(t) = 0.5\ \rho\ V_a(t)^2\ S\ (C_D(t) + C_{D_{tether}}(t)) \tag{3a}$$
$$L(t) = 0.5\ \rho\ V_a(t)^2\ S\ C_L(t) \tag{3b}$$
$$Y(t) = 0.5\ \rho\ V_a(t)^2\ S\ C_Y(t) \tag{3c}$$
$$l(t) = 0.5\ \rho\ (V_a)^2(t)\ S\ b\ C_l(t) \tag{3d}$$
$$m(t) = 0.5\ \rho\ (V_a)^2(t)\ S\ \bar{c}\ C_m(t) \tag{3e}$$
$$n(t) = 0.5\ \rho\ (V_a)^2(t)\ S\ b\ C_n(t) \tag{3f}$$

These forces are expressed in the wind system of coordinates, so they are transformed to the body axis.

3.2.2 Motors' effect

The subindex in T_i and Q_i refers to the rotor position (1: front-right, 3: front-left, 2: back-right, 4: back-left) . The total forces of the motors are presented from (4b) to (4d), while the moments are presented from (4e) to (4f).

$$F_{T_x} = 0 \tag{4a}$$
$$F_{T_y} = 0 \tag{4b}$$
$$F_{T_z}(t) = -(T_1(t) + T_2(t) + T_3(t) + T_4(t)) \tag{4c}$$
$$l_R(t) = -T_1(t) + T_2(t) + T_3(t) - T_4(t) \tag{4d}$$
$$m_R(t) = T_1(t) - T_2(t) + T_3(t) - T_4(t) \tag{4e}$$
$$n_R(t) = Q_1(t) + Q_2(t) + Q_3(t) + Q_4(t) \tag{4f}$$

3.2.3 Dynamic equations

All the different components are included to write the differential equations for the fixed-wing drone. The idea is to follow the approach of the Newton's Laws and express everything in terms of the drone's speeds. Equations from (5a) to (5c) are the expressions needed to calculate the states related to linear movement, while equations ranging from (5d) to (5f) defines the dynamic of the states related to angular movements.

$$\dot{U} = \frac{F_{A_x} + F_{T_x}}{mass}\ +\ g_x\ +\ WQ\ +\ VR \tag{5a}$$
$$\dot{V} = \frac{F_{A_y} + F_{T_y}}{mass}\ +\ g_y\ +\ UR\ +\ WP \tag{5b}$$
$$\dot{W} = \frac{F_{A_z} + F_{T_z}}{mass}\ +\ g_z\ +\ VP\ +\ UQ \tag{5c}$$
$$\dot{P} = (c_1 R + c_2 P)Q\ +\ c_3(l + l_R)\ +\ c_4(n + n_R) \tag{5d}$$
$$\dot{Q} = c_5\ R\ P -\ c_6(P^2 - R^2)\ +\ c_7(m + m_R) \tag{5e}$$
$$\dot{R} = (c_8 P + c_2 R)Q +\ c_4(l + l_R)\ +\ c_9(n + n_R) \tag{5f}$$

The terms c_i in the above equations are related to the inertia of the drone. while the decomposition of the gravity in the body axis is done thanks to the quaternion representation.

3.2.4 Quaternion update

In order to update the quaternion representation, its derivative can be written as follows. Then, the next pose of the drone is obtained by integrating this derivative with the rest of the state's derivates.

$$\dot{q}(t) = 0.5 \begin{bmatrix} -q_1(t) & -q_2(t) & -q_3(t) \\ q_0(t) & -q_3(t) & q_2(t) \\ q_3(t) & q_0(t) & -q_1(t) \\ -q_2(t) & q_1(t) & q_0(t) \end{bmatrix} \begin{bmatrix} P(t) \\ Q(t) \\ R(t) \end{bmatrix} \tag{6}$$

4. Control System

The proposed system is based on a cascade approach, where the closed-loop dynamics at the lowest level are used as the basis for the design of the higher levels. The switching among them is done according to a State machine, explained below. The models for each controller are a linear simplification of the non-linear equations presented before. When the model is a MIMO system, the LQR method [1] is used. On the other hand, if the system is SISO, the Affine Parameterization[1] technique is used.

4.1. State machine

The whole mission consists of 7 Phases, each representing a distinct phase with its problems and, thus, controllers and references as solutions. The first 3 states (**Phase 0 - Take off**, **Phase 1 - Approach sphere's surface** and **Phase 2 - Tether engaging**) and the last one (**Phase 6 - Retraction**) have as characteristic a loose tether, where its length is 10% larger than the drone distance to the generator. Conversely, the other phases present a taut tether. **Phase 3 - Climbing on the sphere** and **Phase 4 - Stabilization** (switching objective points with constant tether length) have a

constant tether length, while in **Phase 5 - Generation** the tether is reeled out due to the lift force. Phase 6 is divided into four parts. Part 1: turning toward the objective point. Part 2: gliding towards the objective point. Part 3: nose down, turn outwards and make the longitudinal axis point toward the opposite objective point by leveraging the yaw angle reference. Part 4: switch to tether angles, taking θ_{tether} to zero and using ϕ_{tether} to control the side-slip angle. The yaw is still used with the same objective that part 3.

4.2. Hovering control

During hovering, the motors are responsible for the attitude and altitude control. In figure 2 it is possible to see how is the control logic. This phase comprises from Phase 0 up to Phase 3; however, the first three of them have a cascade controller with one layer more than the last one. The latter is characterized by a taut tether (*taut tether control*), while the remaining three move with a loose tether (*loose tether control*).

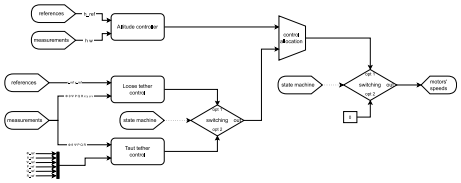

Figure 2: Complete hovering control block diagram

The *altitude controller* is based on a linear dynamical model with three states, the altitude, its derivative and the integration of the error. On the side of *taut tether control*, it has two layers, called *Inner layer* and *Middle layer*. The first one returns a set of references for the motors' angular speeds. The model used for its synthesis is the linear version of equations from (5d) to (5f). On the other hand, the *Middle layer - Euler controller* is in charge of tracking the angular position described by the three Euler angles. The control scheme is presented below.

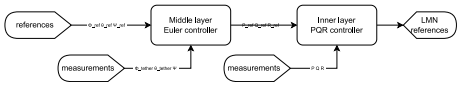

Figure 3: Schematic block diagram of the Taut Tether Control subsystem

The *loose tether control* subsystem includes an inner and middle layer, equal to the ones in the *Taut tether control* subsystem. However, the *loose tether control* subsystem requires another layer in the cascade scheme. The new block scheme is shown in figure 4.

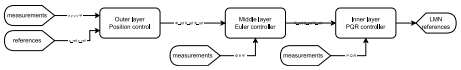

Figure 4: Schematic block diagram of the Loose Tether Control subsystem

The *Outer layer - Position control* is used in the case of having the earth positions as references. For the *position controller*, the desired positions $x_{def}(t)$ and $y_{def}(t)$ are the inputs. The *velocity controller* returns the $\theta(t)$ and $\phi(t)$ necessary to reach certain speed values.

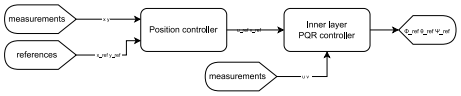

Figure 5: Schematic block diagram of the Position controller

Control allocation - Hovering

With the required moments and the force computed, the motor's speeds are calculated based on the motor's models and the drone's sum of forces and moments. Afterwards, it is necessary to implement a saturation to the angular speed reference to prevent negative values and excess speed.

4.3. Airplane mode control

This control system is enabled from Phase 4 to Phase 6. A cascade controller strategy allows the drone to complete the generation and retraction phase, with the transition in between them. The *Inner layer - attitude controller* is divided into generation and retraction phase. Both of them compute the required aerodynamic moments. The retraction one uses only the Euler angles and their derivatives, while the generation phase adds an integral action on the ψ error.
The *outer layer* is responsible for feeding the references to the inner layer controllers. While its own set of references is related to the Phase that the State machine chooses at any point. During the generation phase, there are two controllers.

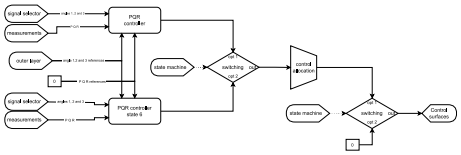

Figure 6: Schematic block diagram of the Inner layer for airplane mode

The first one is for the forward speed, providing references for θ_{tether}. The second one is for the side-slip angle, by computing references for ϕ_{tether}. Both of them leverage the projection of the tether force. The other output is the velocity angle reference.

4.3.1 strategy outline

The retraction phase is the main point of the study of this work. In the next paragraphs, the control scheme is explained. In addition, the four parameters chosen to define the method are presented. The effect of them on the feasibility of the drone reaching the next generation phase is portrayed in some figures. Those four parameters are the *Objective altitude*, which is the amount of altitude to lose from the starting of phase 6 to reach the objective point. It is used to prevent the drone from hitting the ground when turning. The *rate of change* in ψ_{ref} during part three affects how much to drop before changing to part 4 and how much the nose is turning towards the opposite objective point. The *altitude drop* defines much to dive before starting part 4. The *distance to switch* to part 3 in x_{ef} can be explained as the distance the drone must glide past the objective point to switch to part 3. It affects mainly how the tether is engaged. If the tether is engaged too soon or too late, its force will pull the drone too firmly and with an incorrect angle, so the attitude will be so bad it makes it impossible to recover.
In the retraction phase, there are several situations to study. The drone glides towards an objective point during the first and second parts of phase 6. In these parts, the references are computed for the Euler angles. θ is used for adjusting the altitude, ϕ is used for turning and tracking, and ψ is used for keeping β at a minimum. The objective in altitude to finish the gliding is crucial to prevent the drone from hitting the ground during the dive. The changing of it, affecting mainly the θ's reference, can be seen in figure 7.

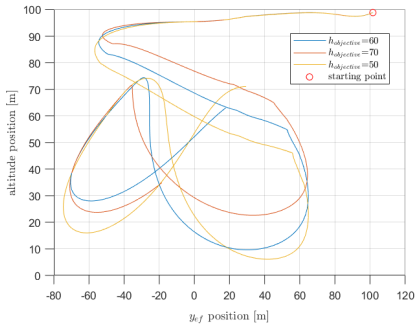

Figure 7: Phase 6 - Effect of change in the Target point's altitude

During the third part, the references are still for the Euler angles. Their objective is different; θ is set to decrease to make the nose point down, ϕ is used to produce a turning towards the opposite direction of the generator, and ψ is used to make the nose point towards the opposite objective point. All of them are changing following a line. Its slope in $\psi_{ref}(t)$ plays an essential role in how much the drone dives and how much it takes for the drone to point to the new Target point. The effect of its variation can be seen in figure 8.

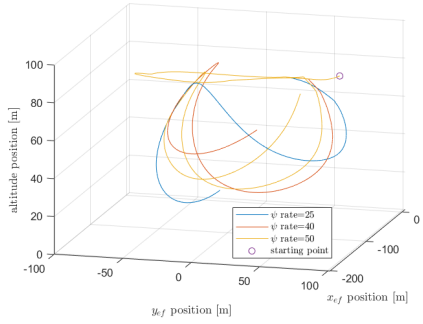

Figure 8: Phase 6 - Effect of change in $\psi(t)$ reference rate of change

How much to dive, in meters, before switching from state 3 to 4 is crucial. It defines how big the linear variations in the references on the Euler angles will reach, resulting in a different attitude at the end. The results can be seen in figure 9.
Finally, the fourth part comes into play to make the tether angles appear and make the last adjustments to the attitude. The reference for ψ is still the same; however, θ_{tether}'s reference is set to linearly decrease to zero, while ϕ_{tether}'s reference is set to the same used during the generation phase.

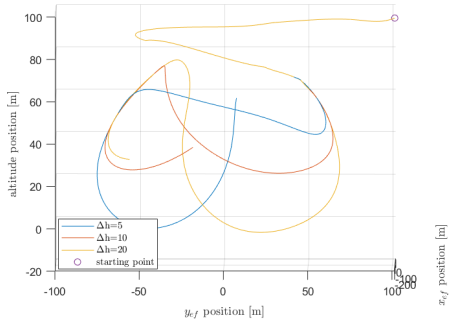

Figure 9: Phase 6 - Effect of change in the dive distance

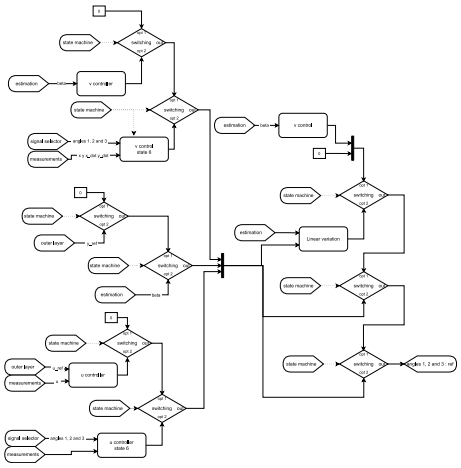

Figure 10: Schematic block diagram of the Outer layer for airplane mode

5. Simulation

Once the unwound tether has reached the maximum permissible length, the transition phase starts. Figure 11 presents the results. It is possible to see how the drone turns, aiming at the Target point 1, and approaches it. Once close enough, the drone dives and turns looking for the Target point 2. When it is in the correct position, it shifts back to Phase 4 and produces the ∞-shape figures that are shown.

6. Conclusions and future developments

To conclude this work, it is possible to see that the methodology proposed enables the possibility of a safe and correct transition by tuning very few parameters. Once the drone has finished Phase 5, with any type of control chosen, the methodology gives some simple rules for the control design of Phase 6.

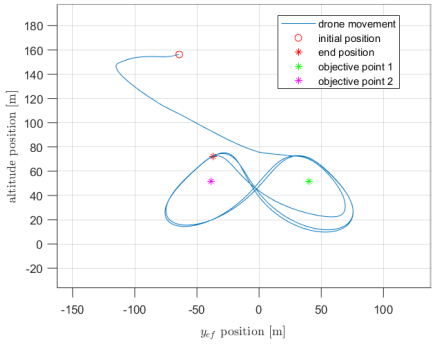

Figure 11: Retraction phase

The future developments that may push this methodology forward are related to optimizing the value of the parameters; one perspective might be the less consumption of energy in control actions. Another possibility is the optimal set of values that permits a transition without the requirement of having to go through Phase 4. Another future development comes from the test and validation of the method in non-ideal wind conditions.

7. Bibliography

References

[1] Graham C. Goodwin, Stefan F. Graebe, and Mario E. Salgado. *CONTROL SYSTEM DESIGN*. Pearson, 2000.

[2] Sebastian Rapp, Roland Schmehl, Espen Oland, and Thomas Haas. Cascaded pumping cycle control for rigid wing airborne wind energy systems. *Journal of Guidance, Control, and Dynamics*, 42:1–18, 06 2019.

[3] ENGIE SA, 2017.

[4] Davide Todeschini, Lorenzo Fagiano, Claudio Micheli, and Aldo Cattano. Control of a rigid wing pumping airborne wind energy system in all operational phases. *Elsevier*, 06 2020.

[5] G. van der Lee Rope Factory, 2022.

8. Acknowledgements

I would like to thank my family, my friends, my girlfriend and Lorenzo Fagiano.